NANO · MICRO small
www.small-journal.com

The Influence of Nanoparticle Shape on Protein Corona Formation

Rahul Madathiparambil Visalakshan, Laura E. González García, Mercy R. Benzigar, Arthur Ghazaryan, Johanna Simon, Agnieszka Mierczynska-Vasilev, Thomas D. Michl, Ajayan Vinu, Volker Mailänder, Svenja Morsbach, Katharina Landfester, and Krasimir Vasilev**

Nanoparticles have become an important utility in many areas of medical treatment such as targeted drug and treatment delivery as well as imaging and diagnostics. These advances require a complete understanding of nanoparticles' fate once placed in the body. Upon exposure to blood, proteins adsorb onto the nanoparticles surface and form a protein corona, which determines the particles' biological fate. This study reports on the protein corona formation from blood serum and plasma on spherical and rod-shaped nanoparticles. These two types of mesoporous silica nanoparticles have identical chemistry, porosity, surface potential, and size in the *y*-dimension, one being a sphere and the other a rod shape. The results show a significantly larger amount of protein attaching from both plasma and serum on the rod-like particles compared to the spheres. Interrogation of the protein corona by liquid chromatography–mass spectrometry reveals shape-dependent differences in the adsorption of immunoglobulins and albumin proteins from both plasma and serum. This study points to the need for taking nanoparticle shape into consideration because it can have a significant impact on the fate and therapeutic potential of nanoparticles when placed in the body.

Nanoparticles (NPs) have become an integral part of many aspects of modern medicine, becoming utility in a wide range of areas such as drug delivery, medical imaging, and diagnostics.[1,2] In this context, mesoporous silica nanoparticles (MSNs) are particularly interesting for medical applications because of their biocompatibility, biodegradability, large surface-to-volume ratio, and tunable pore structures.[3–5] Specifically, MSNs have shown great potential to be applied as drug and biomolecular carriers, in targeted cancer therapies and theranostics.[4] Once administered into the body, the NPs are exposed to the immune system, which may neutralize them prior to reaching the target location.[6] This defense mechanism is part of the foreign body reaction, a process that begins with the random attachment of proteins from the body fluids to the surface of the NPs. In order to create efficient therapies, it is important to understand how NPs interact with proteins and how the composition (and potential impact) of the protein corona that subsequently forms is affected by the key parameters of the NPs.[7] Recent studies have demonstrated how the protein corona composition controls the NPs' nonspecific cellular uptake by immune cells,[8,9] as well as its influence on inflammation and oxidative

Dr. R. Madathiparambil Visalakshan, L. E. González García, Dr. T. D. Michl, Prof. K. Vasilev
Future Industries Institute
School of Engineering
University of South Australia
Mawson Lakes, Adelaide, SA 5095, Australia
E-mail: krasimir.vasilev@unisa.edu.au

Dr. M. R. Benzigar, Prof. A. Vinu
Global Innovative Centre for Advanced Nanomaterials
Faculty of Engineering and Built Environment
The University of Newcastle
Callaghan, NSW 2308, Australia

The ORCID identification number(s) for the author(s) of this article can be found under https://doi.org/10.1002/smll.202000285.

DOI: 10.1002/smll.202000285

Dr. M. R. Benzigar
Graduate School of Biomedical Engineering
The University of New South Wales
Sydney, NSW 2052, Australia

Dr. A. Ghazaryan, Dr. J. Simon, Prof. V. Mailänder, Dr. S. Morsbach, Prof. K. Landfester
Physical Chemistry of Polymers
Max Planck Institute for Polymer Research
Ackermannweg 10, Mainz 55128, Germany
E-mail: landfest@mpip-mainz.mpg.de

Dr. A. Mierczynska-Vasilev
The Australian Wine Research Institute
Waite Precinct
Hartley Grove cnr Paratoo Road, Urrbrae (Adelaide) SA 5064, PO Box 197
Glen Osmond, SA 5064, Australia

Prof. V. Mailänder
Department of Dermatology
University Medical Center of the Johannes Gutenberg-University Mainz
Langenbeckstr. 1, Mainz 55131, Germany

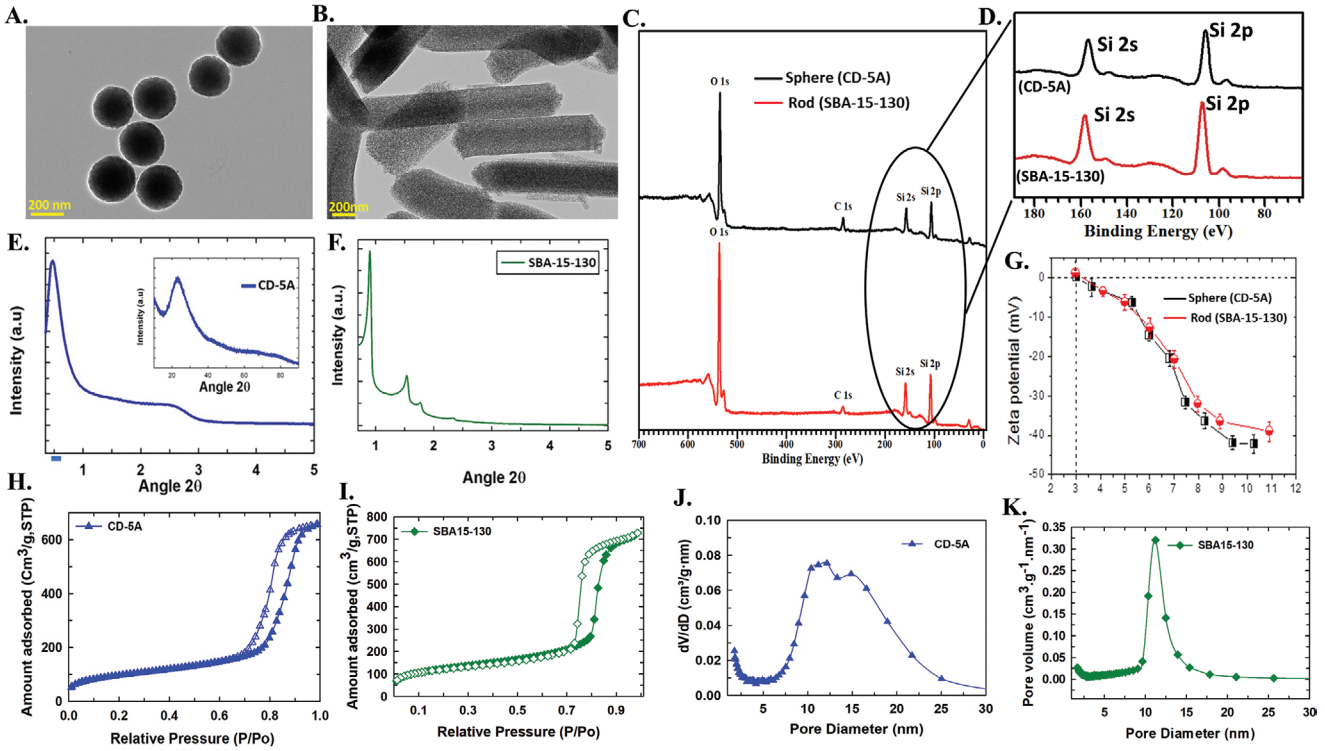

Figure 1. A) TEM images of the sphere (CD-5A) and B) the rod (SBA-15-130St) mesoporous silica NPs. C) XPS survey spectra of rod and sphere MSNs and D) the corresponding high-resolution spectra of Si. E) Low-angle XRD pattern of core–shell NPs, inset shows higher-angle XRD pattern. F) Low-angle XRD pattern of SBA-15-130St synthesized at static condition. G) Zeta potential measurement of rod and sphere MSNs as a function of pH. Nitrogen adsorption-desorption pattern of H) sphere (CD-5A) and I) rod (SBA-15-130St). Pore-size distribution of J) sphere and K) rod MSNs.

stress.[10] Since the protein corona predetermines nanomaterials' biological fate, extensive research has been carried out to understand the factors shaping corona formation[11–13] such as particle size,[14] surface charge,[15] surface chemistry,[16] and biological media composition.[17] These studies point out that the fate of NPs in the body highly depends on the type and amount of adsorbed proteins on their surface.

Recently, it has been demonstrated that the shape of the NPs can also significantly impact their performance in terms of blood circulation time, cellular internalization, bio-distribution, endocytosis by immune cells, and residence time within the cell.[18] As an example, nonspherical particles have been reported to have longer circulation times, reduced phagocytosis by macrophages, and lower cellular uptake than their spherical counterparts.[19–21] It has also been shown that specific cells can be selectively targeted by controlling the shape of NPs.[22] Studies with Hela and Caco-2 cells have shown high efficiency in cellular uptake of rod-shaped particles.[23,24] Another study of MSNs with spherical and tubular morphology involving Chinese hamster ovary and fibroblast cells illustrated that cellular uptake was morphology and cell line independent, even though, the endocytosis rate was greater for spheres compared to rod-shaped particles.[25] Interestingly, recent hemolysis studies indicate that MSNs morphology affects the hemolytic activity in red blood cells and cytotoxicity is reduced in the presence of serum proteins, albeit using only a few selected proteins.[5] These studies point to the possibility of using NP morphology as a tool to engineer the next generation of drug delivery and theranostic vehicles. However, as with all biomaterials, upon administration, the biological fate of NPs depends on the rapidly forming protein corona.[8] Yet, the relationship between NP shape and protein corona formation is still unknown. However, this knowledge is vital for the design of the next generation of nanomaterials that intelligently interact with the constituents of tissue and biological fluids for the detection and treatment of many diseases.

To address this challenge, we prepared two chemically identical mesoporous silica NPs of comparable size in one of the dimensions that was either rod- or sphere-shaped and exposed them to human serum and plasma. The two types of MSNs are shown in the transmission electron microscopy (TEM) images in **Figure 1**A,B. Rod-shaped MSNs (SBA-15-130st) were prepared under static conditions using a soft templating approach in an acidic condition as previously reported.[26,27] Core–shell spherical MSNs (CD-5) were specifically synthesized for this study. The TEM images in Figure 1A show that CD-5 had spherical morphology with particle diameters of 270 ± 20 nm. Rod-like SBA-15 had nearly identical size in the *y*-dimension (290 ± 30 nm) as CD-5 but an average length (*x*-dimension) of 1100 nm (Figure 1B). Further characterization by SEM presented in Figure S1, Supporting Information, confirms the shape, size, and uniformity of both NPs. The surface chemical composition of both NPs obtained from *x*-ray photoelectron spectroscopy (XPS) analysis is shown in Figure 1C and the high-resolution spectra of silica in Figure 1D. Within the experimental uncertainty of XPS, the atomic percentage of carbon, oxygen, and

Table 1. The atomic composition of the surface of the NPs as determined via XPS. All XPS data contain a standard error of 5%.

Shape	O [%]	C [%]	Si [%]
Sphere (CD-5A)	50.2	8.7	40.9
Rod (SBA-15-130St)	50.5	8.2	41.1

silicon in the outermost 10 nm of the surface is nearly identical for both types of NPs (**Table 1**) as well as the oxidation state of Si. Additional analysis was conducted by SEM EDAX mapping (Figures S2 and S3, Supporting Information), which further confirm that both NPs had identical surface chemistry.

The structure of the prepared core–shell spherical NPs (CD-5A) was confirmed by powder X-ray diffraction (XRD) analysis. Figure 1E shows a low-angle powder XRD pattern for core–shell MSNs. The XRD pattern exhibits a major high-ordered peak at the 2θ of 0.5° and a second minor broader peak around the 2θ of 2.5°, confirming the ordered mesoporous structure of sphere-shaped NPs (CD-5A). The wide-angle XRD pattern (Figure 1E, inset) displays a peak ≈23°, determining the amorphous nature of the material. Figure 1F presents a low-angle powder XRD pattern for the rod-shaped particles (SBA-15-130st) that exhibits three well-ordered peaks that can be indexed as (100), (110), and (200) reflection planes on a 2D hexagonal lattice with p6mm symmetry.[26,28–30] Surface charge is known to be an important regulator of protein interaction with NPs. Figure 1G shows that CD-5 and SBA-15 have almost the same zeta potential of –20 mV at pH 7. The CD-5 material exhibits a type IV isotherm with a sharp capillary condensation step and an H1 hysteresis loop, which is typical of mesoporous materials exhibiting well-ordered cylindrical pores with large pore diameter (Figure 1H). The surface area of this material was found to be 351.3 $m^2\ g^{-1}$ with a pore diameter of 11.9 nm and pore volume being 0.97 $cm^3\ g^{-1}$ (Figure 1J). The structure of the SBA-15-130St material is similar to that of pure SBA-15. The shape of the particles is rectangular with a surface area of 446.56 $m^2\ g^{-1}$ and pore diameter of 11.25 nm with a pore volume of 1.12 $cm^3\ g^{-1}$ (Figure 1I,K) that is consistent with previous reports.[27,29] The comprehensive analysis of CD-5 and SBA-15 demonstrates that the two NP samples have nearly identical pore size, chemical composition, and zeta potential but only differ by their shape—one being spherical and the other rod-shaped, both having 1D of comparable size.

To study the effect of NPs' shape on protein corona formation (**Figure 2**A), we incubated the spherical and rod-shaped MSNs in human serum and plasma for 1 h with continuous agitation using a rotating shaker. In order to account for the differences in rod-shaped and spherical particle surface area and to ensure reproducibility, 0.05 m^2 of sample surface area was exposed to 1 mL of serum and plasma. The samples were then centrifuged and washed three times with phosphate-buffered saline (PBS) to remove any unbound proteins. Subsequently, the total protein adsorption was determined via a colorimetric protein quantitation assay (Pierce BCA protein assay). The composition of the protein corona was analyzed by sodium dodecyl

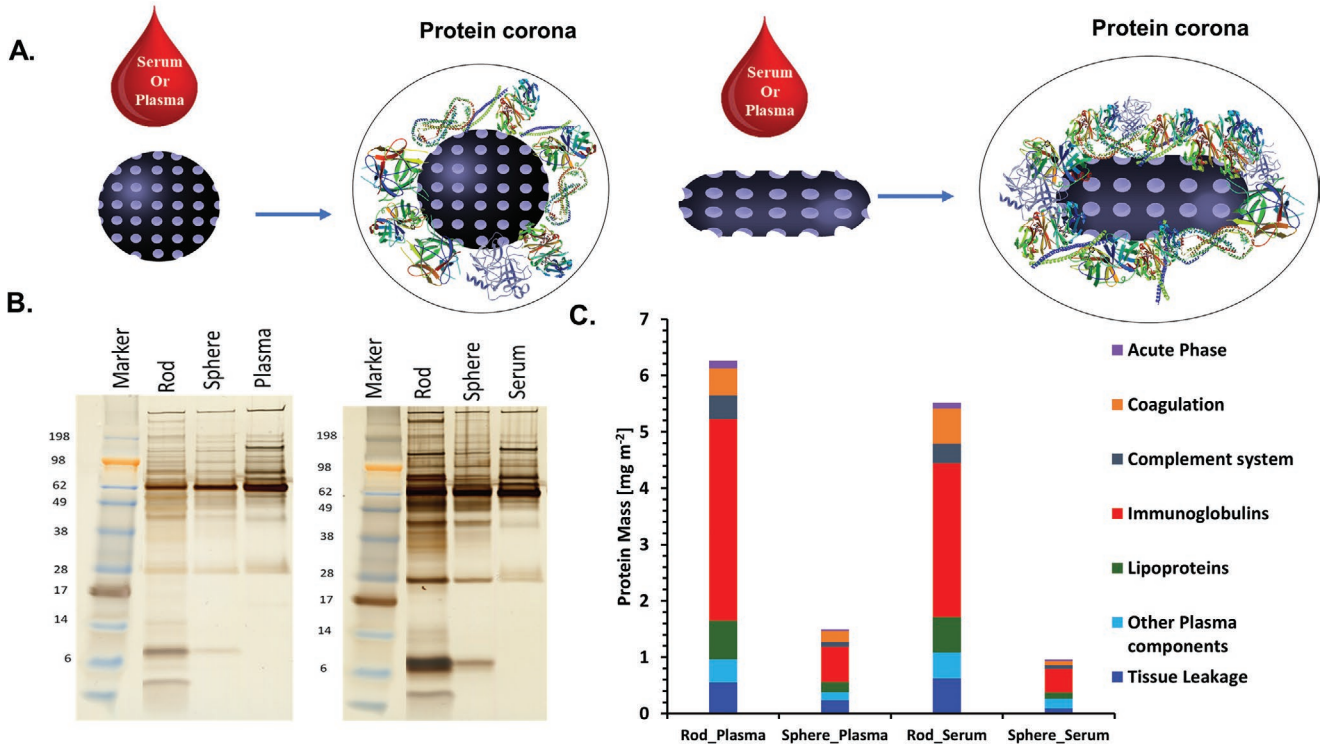

Figure 2. A) Schematic illustration of the fate of MSN's, blood–NP interaction leading to protein adsorption and protein corona formation around the NPs. B) Gel electrophoresis: the visual representation of protein corona contents based on molecular weights. C) Quantification of human plasma and serum protein mass adsorbing to the mesoporous NPs along with the classification of protein corona components identified by quantitative LC-MS. Identified proteins were grouped according to their function in the biological process.

sulfate-polyacrylamide gel electrophoresis (SDS–PAGE) and label-free liquid chromatography-mass spectrometry (LC-MS). The molecular weight distribution pattern of proteins and protein complexes shown in the SDS–PAGE images (Figure 2B) reveal that the corona is composed of a large number of different constituents. The results presented in Figure 2C show that there is a significantly higher amount of proteins adsorbed onto the rod-shaped particles compared to those having a spherical shape. Detailed quantification of the amount of proteins adsorbed on a per particle basis is presented in Figure S4 and Table S1, Supporting Information. This trend was observed for both serum and plasma, the increase being threefold for plasma and fourfold for serum. This result is in agreement with a published study by Gagner et al. who reported similar results with individual proteins, that is, lysozyme and α-chymotrypsin, attached in greater amounts on gold nanorods compared to gold nanospheres.[31]

These findings may be explained by taking into consideration the geometry of the NPs. The rod-shaped NPs possess two dimensions and average curvatures that are defined by the circumference of the rod and a relatively flat surface along the cylindrical/longitudinal axis. It might be possible that the longitudinal axis of the rods, where the curvature is only 1D, allows for greater protein packing density resulting in an overall larger protein amount to be adsorbed. For small proteins with dimensions less than the diameter of the rod-shaped NP's facets, this surface can be considered as a relatively flat surface. Therefore, an increased lateral interaction on the relatively "flat" cylindrical surface may facilitate a higher packing density of proteins adsorbed on rod-shaped NPs when compared to spherical NPs.[31] Previous studies with spherical NPs of different sizes also displayed an inverse relationship between protein adsorption and surface curvature.[32] Similarly, a high degree of curvature may prevent protein–protein interaction and interfere with the efficient close packing on the NP surfaces.[33] Further studies at the single protein level, which allow for revealing potential conformational changes of proteins on curvatures in one and two dimensions, are required to fully unravel the observed phenomena.

LC-MS was employed to identify and quantitatively determine the individual proteins forming the corona. We further grouped the constituents of the protein corona in terms of their functions into acute phase, coagulation, complement, lipoproteins, immunoglobulins, tissue leakage, and others (Figure 2C). The exact constituents of each group are shown in Table S2, Supporting Information. Overall, the type of adsorbed proteins does not appear to be significantly different for both types of NPs, but the amount of protein adsorption varied between the spherical and rod-shaped particles. Immunoglobulins were the most abundant proteins in the corona adsorbed from both serum and plasma. Rod-shaped particles attracted a greater amount of immunoglobulins compared to spheres with 57% (3.57 mg m^{-2}) in the plasma and 50% (2.7 mg m^{-2}) in the serum corona. Spherical particles adsorbed 42% (0.62 mg m^{-2}) and 45% (0.43 mg m^{-2}) of immunoglobulins from plasma and serum, respectively. All other protein groups composed nearly identical fractions of the protein corona formed on rods and spheres and did not exceed 20% for both plasma and serum.

The most abundant proteins found in the corona formed from plasma and serum on the surface of the NPs are summarized in a heat map and presented in **Figure 3**. The heat map shows several interesting facts. Notably, on one side, the corona of both types of NPs contained relatively small amounts of albumin (12% or less) compared to serum and plasma controls, where albumin is the most abundant protein. On another hand, a high quantity (30% or above) of Ig gamma-2 chain C region was concentrated on the surface of the NPs relative to the concentration of this protein in plasma and serum. These findings demonstrate the selective protein adsorption profile for MSNs. The amount of Ig gamma-2 chain C region was significantly greater on rod-shaped compared to spherical particles for both serum (36% vs 30%) and plasma (38% vs 30%) corona. Additionally, a similar trend was also found for immunoglobulin heavy variable 3-66 where a higher amount adsorbed onto rods (10% from plasma and 9% from serum) compared to spheres (7% from plasma and 8% from serum). Figure 3 also indicates that a higher amount of albumin was bound to spheres compared to the rods after incubation in serum (12% vs 2%). A similar trend was detected for the plasma corona, that is, the amount of albumin adsorbed on the sphere and rod being 3% and 1%, respectively. Rod-shaped particles attracted more complement C1s protein than sphere particles for plasma corona (4% vs 2%). However, after serum incubation, the amount of complement C1s was identical on both types of particles. The corona also appeared to be rich in apolipoprotein B-100 with an identical adsorption pattern for both particles. Apolipoprotein B-100 is beneficial for the targeted delivery of NPs to the brain and widely used to functionalize NPs for this purpose.[34–36]

As shown in Figure 1E,F, a distinctive characteristic between the spherical and rod-shaped mesoporous silica NPs is their crystallinity. While the atoms in spherical silica NPs are packed in an amorphous structure, rod-shaped NPs have their atoms arranged in a primitive hexagonal net crystalline structure. The arrangement of atoms in a solid material is directly related to the surface energy that can be defined as the energy cost per unit area of the new surface formed. Because of their distinct structures, the two shapes of mesoporous silica NPs have different surface energies.[37,38] Studies suggest that various chemical species have preferential interactions with specific crystal planes as a result of the different surface energies.[39] As steric and chemical factors also play an important role in protein adsorption phenomena, it would be reasonable to assume that proteins, such as immunoglobulins, can also have preferential interactions with specific structures in nanomaterials.

The function of immunoglobulins is the activation of the immune defense system.[40] The significantly greater amount of immunoglobulins binding to the rod-like particles suggests that NPs with nonspherical shapes may trigger stronger immune responses. These results reveal a complex pattern of recognition on spherical and rod-shaped entities. Thus, it may be possible that specific sets of proteins specialize in clearing foreign objects dependent on their shapes. Since it is known that the protein corona formation strongly influences the retention, transport, and phagocytosis of NPs,[41] the enrichment of opsonins such as immunoglobulins and complement proteins may induce macrophage recognition and phagocytosis, leading to faster removal from the body.[42,43] This

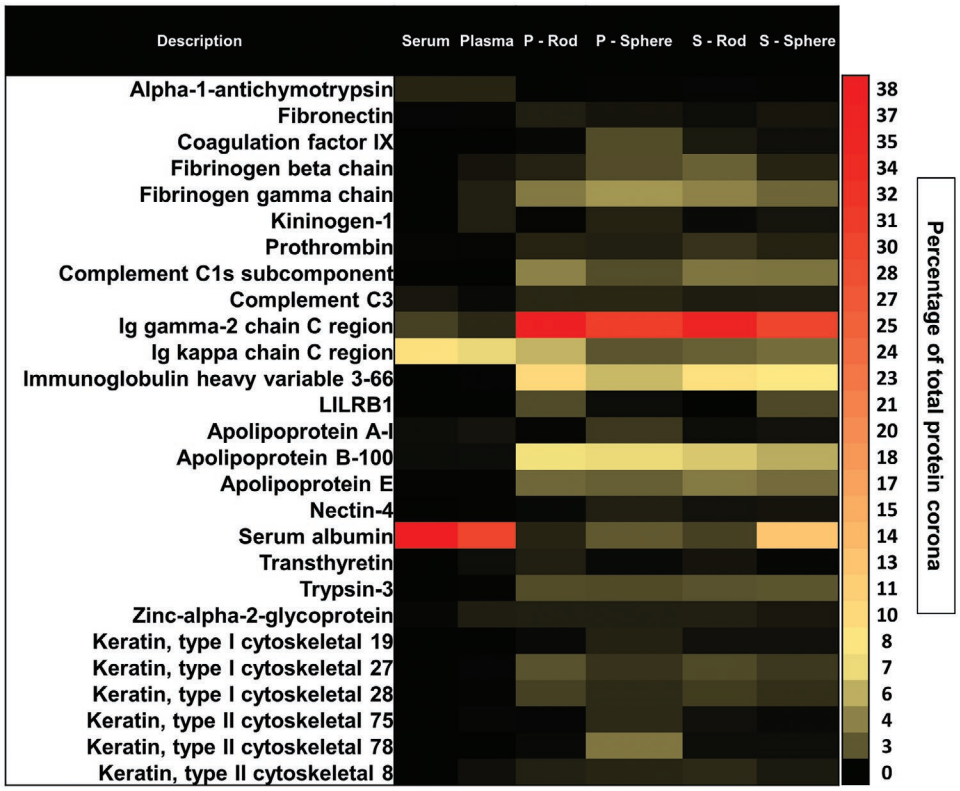

Figure 3. Heat map of the most abundant proteins in serum and plasma as well as in the protein corona of the sphere- and rod-shaped MSNs determined by proteomic mass spectrometry. Values were calculated from the molar masses of each protein identified by LC-MS. Only those proteins that constitute more than 1% of the protein corona on each of the surfaces are shown in the heat map.

immunoglobulin-triggered macrophage recognition could also lead to the accumulation of NPs in the liver and spleen, which may be useful for targeted delivery to these organs.[44] It is also important to note that the corona enriched with dysopsonins such as albumin could lead to an extended circulation time in the body.[41,42]

Collectively, we present protein corona formation studies from both serum and plasma, on spherical and rod-shaped NPs. We prepared two types of mesoporous silica NPs that had identical chemistry, porosity, surface potential, and size in *y*-dimension, one being a sphere and the other a rod-shaped. We found a significantly larger amount of protein attaching from plasma and serum on the rod-like particles compared to the spheres. Analysis of the protein corona by LC-MS and SDS–PAGE revealed very low amounts of adsorbed abundant proteins such as albumin and fibrinogen. We also found shape-dependent differences in the adsorption of immunoglobulin and albumin from both serum and plasma. Our results indicate that the shape of the object is a key factor that attracts specific proteins used by the immune system to recognize and clear foreign entities. These findings point to the need for further detailed studies focusing on understanding of the specific protein adsorption patterns on NPs of different shapes and the conformational state of these proteins. Understanding these phenomena can have a profound implication on how we design NPs for medical therapies and may help the design of more efficient and targeted therapies.

Experimental Section

Synthesis of SBA-15-130st (Rod): The SBA-15, mesoporous silica material, was prepared under static condition using the soft templating approach in an acidic condition.[26,28] In a typical synthesis, 4 g of non-ionic surfactant pluronic P-123, a triblock copolymer with the molecular formula $EO_{20}PO_{70}EO_{20}$, was added with 30 mL of double distilled water and stirred continuously for 3 h. Subsequently, 120 g of 2 M HCl was added, and then the temperature was gradually increased to 40 °C, and the sample was further stirred for 2 h. Nine grams of tetraethyl orthosilicate (98%) was added dropwise, and the mixture was stirred for 20 min. Stirring was discontinued afterward, and the sample was allowed to rest for the next 24 h at a constant temperature of 40 °C. Finally, the milky solution obtained was transferred to a Teflon-lined autoclave and kept under the hydrothermal condition at 130 °C for the next 48 h. The resulting product was filtered with hot deionized water and washed three times with the same solution. The final precipitate obtained after thorough percolation was dried at 100 °C for 6 h and then calcined at 540 °C for 12 h for the removal of the leftover polymeric surfactant and any impurities present. The obtained samples were labeled SBA-15-130st, where st denotes the static synthesis condition.

Synthesis of Core–Shell NP CD-5A (Sphere): In a typical synthesis, 0.1 g of F127 pluronic surfactant ($(EO)_{106}(PO)_{70}(EO)_{106}$) was weighed and dissolved in 20 mL of tetrahydrofuran. Then, 0.2 g of hexadecyltrimethylammonium bromide was dissolved in 80 mL of deionized water, and 3 mL of ammonia solution was slowly mixed with the above solution and stirred for 10 min at room temperature. Subsequently, 1 g of tetraethyl orthosilicate (98%) was added dropwise, and the stirring was continued for 24 h at room temperature. The milky solution obtained after 24 h was collected and allowed for aging under the hydrothermal condition at the temperature of 130 °C for another 24 h. The precipitate formed was then centrifuged at 8000 rpm for 10 min, and the pellet was collected. Finally, the pellet was

dried at 70 °C for 6 h and allowed for calcination at 550 °C, and the final product was collected as a white powder.

Protein Corona Preparation: Human blood plasma (heparin anticoagulant) and serum were purchased from Innovative Research, Inc. In order to remove any aggregated proteins, the samples were centrifuged for 1 h at 20 000 × *g* before usage. Each NP solution prepared in MilliQ water was incubated with plasma and serum in three replicates. Based on the surface area calculated from BET, the NP surface concentration to the serum and plasma was kept contestant at 0.05 m^2 per 1 mL and incubated with 1 mL human plasma and serum for 1 h with constant agitation. The particles were separated from the supernatant by centrifugation at 20 000 × *g* for 1 h. The particle pellet was resuspended in PBS and washed by three-centrifugation steps at 20 000 × *g* for 1 h and subsequent redispersion in PBS. Before the last washing step, the dispersion was transferred into a new tube. After the final wash, 150 µL of SDS-Tris-HCl buffer (40 mg SDS+125 µL Tris-HCl+MilliQ water up to a total of 2 mL) was added and incubated by shaking at 95 °C for 15 min. Final centrifugation was performed for 1 h at 4 °C at 20 000 × *g* to isolate the proteins. The total protein concentrations were determined using Pierce 660 nm protein assay according to the manufacturer's instruction.

Sodium Dodecyl Sulfate–Polyacrylamide Gel Electrophoresis: A total of 16.25 µL of the protein sample was mixed with 6.25 µL NuPAGE LDS sample buffer and 2.5 µL NuPAGE sample reducing agent and applied onto a NuPAGE 10% Bis-Tris protein gel (all Novex, Thermo Fisher Scientific). The electrophoresis was carried out in NuPAGE MES SDS running buffer at 150 V for 1.5 h with SeeBlue Plus2 Pre-Stained Standard (Invitrogen) as a molecular marker. The gel was stained using the Pierce Silver Stain Kit (Novex, Thermo Fisher Scientific).

LC-MS Analysis: Quantitative analysis of protein samples was performed using a nanoACQUITY UPLC system coupled with a SynaptG2-Si mass spectrometer (Waters Corporation). Tryptic peptides were separated on the nanoACQUITY system equipped with a C18 analytical reversed-phase column (1.7 µm, 75 µm × 150 mm, Waters Corporation) and a C18 nanoACQUITY Trap Column (5 µm, 180 µm × 20 mm, Waters Corporation).

Supporting Information

Supporting Information is available from the Wiley Online Library or from the author.

Acknowledgements

K.V. thanks ARC for DP15104212 and DP180101254, NHMRC for fellowship APP1122825 and project grant APP1032738, and the Alexander von Humboldt Foundation for Fellowship for Experienced Researchers. The authors acknowledge the facilities, scientific, and technical assistance of Microscopy Australia at the University of South Australia, a facility that is funded by the University of South Australia, the State and Federal Governments.

Conflict of Interest

The authors declare no conflict of interest.

Keywords

bio-nanoparticle interactions, mesoporous nanoparticles, nanoparticle shape, protein adsorption, protein corona, rod shape, sphere shape

Received: January 15, 2020
Revised: April 2, 2020
Published online:

[1] R. A. Petros, J. M. DeSimone, *Nat. Rev. Drug Discovery* **2010**, *9*, 615.
[2] W. H. De Jong, P. J. Borm, *Int. J. Nanomed.* **2008**, *3*, 133.
[3] Y. Wang, Q. Zhao, N. Han, L. Bai, J. Li, J. Liu, E. Che, L. Hu, Q. Zhang, T. Jiang, *Nanomedicine* **2015**, *11*, 313.
[4] F. Tang, L. Li, D. Chen, *Adv. Mater.* **2012**, *24*, 1504.
[5] Z. Ma, J. Bai, Y. Wang, X. Jiang, *ACS Appl. Mater. Interfaces* **2014**, *6*, 2431.
[6] H. J. Johnston, G. Hutchison, F. M. Christensen, S. Peters, S. Hankin, V. Stone, *Crit. Rev. Toxicol.* **2010**, *40*, 328.
[7] R. García-Álvarez, M. Hadjidemetriou, A. Sánchez-Iglesias, L. M. Liz-Marzán, K. Kostarelos, *Nanoscale* **2018**, *10*, 1256.
[8] S. Schöttler, G. Becker, S. Winzen, T. Steinbach, K. Mohr, K. Landfester, V. Mailänder, F. R. Wurm, *Nat. Nanotechnol.* **2016**, *11*, 372.
[9] S. Ritz, S. Schöttler, N. Kotman, G. Baier, A. Musyanovych, J. Kuharev, K. Landfester, H. Schild, O. Jahn, S. Tenzer, V. Mailänder, *Biomacromolecules* **2015**, *16*, 1311.
[10] V. Escamilla-Rivera, M. Uribe-Ramirez, S. González-Pozos, O. Lozano, S. Lucas, A. De Vizcaya-Ruiz, *Toxicol. Lett.* **2016**, *240*, 172.
[11] S. Tenzer, D. Docter, J. Kuharev, A. Musyanovych, V. Fetz, R. Hecht, F. Schlenk, D. Fischer, K. Kiouptsi, C. Reinhardt, *Nat. Nanotechnol.* **2013**, *8*, 772.
[12] J. Lazarovits, Y. Y. Chen, E. A. Sykes, W. C. Chan, *Chem. Commun.* **2015**, *51*, 2756.
[13] H. Moustaoui, J. Saber, I. Djeddi, Q. Liu, D. Movia, A. Prina-Mello, J. Spadavecchia, M. L. de la Chapelle, N. Djaker, *Nanoscale* **2019**, *11*, 3665.
[14] S. Tenzer, D. Docter, S. Rosfa, A. Wlodarski, J. Kuharev, A. Rekik, S. K. Knauer, C. Bantz, T. Nawroth, C. Bier, *ACS Nano* **2011**, *5*, 7155.
[15] C. Gräfe, A. Weidner, M. vd Lühe, C. Bergemann, F. H. Schacher, J. H. Clement, S. Dutz, *Int. J. Biochem. Cell Biol.* **2016**, *75*, 196.
[16] A. Kurtz-Chalot, C. Villiers, J. Pourchez, D. Boudard, M. Martini, P. N. Marche, M. Cottier, V. Forest, *Mater. Sci. Eng., C* **2017**, *75*, 16.
[17] S. Schöttler, K. Klein, K. Landfester, V. Mailänder, *Nanoscale* **2016**, *8*, 5526.
[18] E. C. Cho, L. Au, Q. Zhang, Y. Xia, *Small* **2010**, *6*, 517.
[19] Y. Geng, P. Dalhaimer, S. Cai, R. Tsai, M. Tewari, T. Minko, D. E. Discher, *Nat. Nanotechnol.* **2007**, *2*, 249.
[20] L. Florez, C. Herrmann, J. M. Cramer, C. P. Hauser, K. Koynov, K. Landfester, D. Crespy, V. Mailänder, *Small* **2012**, *8*, 2222.
[21] J. A. Champion, S. Mitragotri, *Proc. Natl. Acad. Sci. USA* **2006**, *103*, 4930.
[22] M. Janát-Amsbury, A. Ray, C. Peterson, H. Ghandehari, *Eur. J. Pharm. Biopharm.* **2011**, *77*, 417.
[23] S. E. Gratton, P. A. Ropp, P. D. Pohlhaus, J. C. Luft, V. J. Madden, M. E. Napier, J. M. DeSimone, *Proc. Natl. Acad. Sci. USA* **2008**, *105*, 11613.
[24] D. S. Karaman, D. Desai, R. Senthilkumar, E. M. Johansson, N. Råtts, M. Odén, J. E. Eriksson, C. Sahlgren, D. M. Toivola, J. M. Rosenholm, *Nanoscale Res. Lett.* **2012**, *7*, 358.
[25] B. G. Trewyn, J. A. Nieweg, Y. Zhao, V. S.-Y. Lin, *Chem. Eng. J.* **2008**, *137*, 23.
[26] M. R. Benzigar, S. Joseph, H. Ilbeygi, D. H. Park, S. Sarkar, G. Chandra, S. Umapathy, S. Srinivasan, S. N. Talapaneni, A. Vinu, *Angew. Chem.* **2018**, *130*, 578.
[27] K. S. Lakhi, A. V. Baskar, J. S. Zaidi, S. S. Al-Deyab, M. El-Newehy, J.-H. Choy, A. Vinu, *RSC Adv.* **2015**, *5*, 40183.
[28] M. R. Benzigar, S. Joseph, A. V. Baskar, D. H. Park, G. Chandra, S. Umapathy, S. N. Talapaneni, A. Vinu, *Adv. Funct. Mater.* **2018**, *28*, 1803701.
[29] K. S. Lakhi, D.-H. Park, G. Singh, S. N. Talapaneni, U. Ravon, K. Al-Bahily, A. Vinu, *J. Mater. Chem. A* **2017**, *5*, 16220.

[30] M. R. Benzigar, S. N. Talapaneni, S. Joseph, K. Ramadass, G. Singh, J. Scaranto, U. Ravon, K. Al-Bahily, A. Vinu, *Chem. Soc. Rev.* **2018**, *47*, 2680.
[31] J. E. Gagner, M. D. Lopez, J. S. Dordick, R. W. Siegel, *Biomaterials* **2011**, *32*, 7241.
[32] R. M. Visalakshan, A. A. Cavallaro, M. N. MacGregor, E. P. Lawrence, K. Koynov, J. D. Hayball, K. Vasilev, *Adv. Funct. Mater.* **2019**, *29*, 1807453.
[33] S. Lindman, I. Lynch, E. Thulin, H. Nilsson, K. A. Dawson, S. Linse, *Nano Lett.* **2007**, *7*, 914.
[34] J. Kreuter, T. Hekmatara, S. Dreis, T. Vogel, S. Gelperina, K. Langer, *J. Controlled Release* **2007**, *118*, 54.
[35] J. Kreuter, D. Shamenkov, V Petrov, P. Ramge, K. Cychutek, C. Koch-Brandt, R. Alyautdin, *J. Drug Targeting* **2002**, *10*, 317.
[36] J. Kreuter, *J. Microencapsulation* **2013**, *30*, 49.
[37] R. D. Schulman, M. Trejo, T. Salez, E. Raphaël, K. Dalnoki-Veress, *Nat. Commun.* **2018**, *9*, 982.
[38] R. Tran, Z. Xu, B. Radhakrishnan, D. Winston, W. Sun, K. A. Persson, S. P. Ong, *Sci. Data* **2016**, *3*, 160080.
[39] M. Grzelczak, J. Pérez-Juste, P. Mulvaney, L. M. Liz-Marzán, *Chem. Soc. Rev.* **2008**, *37*, 1783.
[40] A. Lesniak, F. Fenaroli, M. P. Monopoli, C. Åberg, K. A. Dawson, A. Salvati, *ACS Nano* **2012**, *6*, 5845.
[41] B.-J. L. Van Hong Nguyen, *Int. J. Nanomed.* **2017**, *12*, 3137.
[42] R. Cai, C. Chen, *Adv. Mater.* **2019**, *31*, 1805740.
[43] V. P. Vu, G. B. Gifford, F. Chen, H. Benasutti, G. Wang, E. V. Groman, R. Scheinman, L. Saba, S. M. Moghimi, D. Simberg, *Nat. Nanotechnol.* **2019**, *14*, 260.
[44] H. Gao, Q. He, *Expert Opin. Drug Delivery* **2014**, *11*, 409.